

Received: 06 April 2023 / Accepted: 17 May 2023 / Published online: 22 May 2023

*drilling, burr, tool geometry,
clean drilling, one shot drilling,
vibration assisted drilling*

Stephan KRALL¹, Markus PRIEBNITZ^{1*},
Christian BAUMANN¹, Peter BRANDT¹,
Friedrich BLEICHER¹

AVOIDANCE OF DRILL CAP FORMATION IN CFRP-TITANIUM STACK MATERIALS BY USING VIBRATION ASSISTED DRILLING WITH DEFINED COUPLING OF THE OSCILLATION

Drilling of rivet holes in stacked materials consisting of CFRP and Ti-6Al-4V still represents unique challenges. It is common practice to drill the material layers using one single tool. When exiting the final metallic layer, formation of a drill cap usually leads to undesirable burrs and debris, requiring manual post-processing. In this work, a drilling process to avoid drill caps is presented. This is realized using low frequency high amplitude vibration assisted drilling with defined coupling of the rotational speed and the axial oscillations. Drilling parameters and their impact on the quality of the drilled hole in the metallic layer are also investigated. It is found that drill tip geometries and process parameters need to be tuned together to achieve a stable and repeatable process for drill cap avoidance. A highly sensorized experimental setup with multi-sensor systems including high-speed and thermal imaging was used for process evaluation.

1. INTRODUCTION

In modern aerospace design, materials like titanium alloys or CFRP allow for weight savings, thereby increasing the carrying capacity of aircraft. This is one of the reasons why a high percentage of the structure of new aircraft is made up of those materials. Over the last 30 years, the proportion of CFRP materials has increased by a factor of 5–6 [1]. Figure 1 shows the material breakdown of the Airbus A350-900 XWB. Titanium and composite structures make up over two thirds of the used materials [2]. Especially in the area of the wings, a stacked arrangement of CFRP and titanium is common. The layers are riveted together, which dictates the need for rivet holes. In one wing of a commercial aircraft, about 40 000 rivets can be found [3]. Currently the drilling process or drill countersinking process is one of the most important processes for the production of aerospace structures.

¹ IFT - Institute for Production Engineering and Photonic Technologies, TU Wien, Austria

* E-mail: markus.priessnitz@tuwien.ac.at

<http://doi.org/10.36897/jme/166274>



Fig. 1. Material ratios in modern aircraft [2]

When drilling rivet holes, the combination of CFRP and titanium presents several challenges due to the diametrically opposed machining conditions for CFRP and titanium. The use of hybrid materials (stacks) made of CFRP and metals leads to additional challenges for the drilling process [4]. While the cutting parameters can be adapted to the respective material layer, a compromise has to be found with respect to the tool, since different cutting materials, geometries or coating can lead to optimum borehole qualities in the different layers [5, 6]. Tool geometries that lead to good qualities within the overall stack may not be optimal, especially for the last metal layer. Thus, the optimization of burr formation at the hole exit is a major challenge in the course of machining multilayer structures next to tool performance. This challenge is particularly acute for the titanium alloy (Ti6-Al-4V), which is most commonly used in aircraft components. Due to the low thermal conductivity of the titanium material, 1000°C can be reached at the cutting edge. This high temperature is responsible for large burrs on both the entry and exit sides, as well as enormous tool wear [7]. Effects of excessive burr can be reflected in a reduction of fatigue life. For this reason, a deburring operation prior to plate assembly is required as a corrective measure, which increases the time for the entire assembly process by almost 30% [8]. Equally relevant are the chips generated in the metal layers of the composite. Compared to other processes, the confined space in the flutes of the drill is of crucial importance in chip evacuation. As a result of inadequate chip evacuation, the chips scratch the surface of the hole, leading to a deteriorated surface finish [9]. With regard to a CFRP-Ti stack, the high temperatures and insufficient chip evacuation also result in problems in the CFRP matrix. Diameter variations and thermal damage to the epoxy resin are not uncommon [10]. Common solutions are “multi-shot” drilling strategies, in which a hole is drilled in several steps (one or more pre-drilling operations and optional reaming) [11]. To prevent damage and remove chips from the flutes, so-called pecking cycles can also be used. Here, chip breaking is forced by a targeted interruption of the feed and a complete or partial retraction of the tool from the hole. In this way, the flutes are emptied and are free of chips for the next cycle section. Although such methods are quite effective, they are inherently associated with a significant increase in cycle times. Approaches by tool manufacturers to reduce the process times with modified drill geometries show first improvements in the direction of “one-shot drilling”, the continuous, cycle-free generation of a drill hole [12, 13]. Building on this, the company Boeing has also taken the first steps towards the realization of “one-up assembly” processes based on rigid drilling platforms that can only be used for a specific application and do not involve disassembly of the structures for cleaning or deburring work [14]. One-up assembly describes a manufacturing process, where the disassembly step can be eliminated. This requires an excellent machining result which ensures repeatable high quality [15]. Boxed in structures like flaps are still problematic

because of chip and lubricant and/or coolant accumulation behind the drill exit, strict foreign object damage (FOD)-free requirements and restricted access for cleaning. The interest in developing new methods to overcome the challenges associated with conventional drilling techniques is on the rise. In this context, vibration assisted drilling (VAD) has emerged as a recent and promising technique that offers significant advantages in terms of productivity [16, 17] and tolerance levels of drilled holes [18, 19]. This includes improved chip-breaking [20], reduced process temperatures [21, 22], as well as improved tool life [23]. VAD employs a controlled harmonic motion to superimpose the feed rate and create an intermittent cutting state [24]. This technique effectively reduces the average cutting force and improves the chip removal process [25], leading to higher cutting speeds and longer tool life. Additionally, VAD allows for better control of the drilled hole's dimensional accuracy and surface finish. By combining VAD, with a distinct exit strategy (a specialized parameter set) optimized for chip removal by destruction of the drill cap as well as coolant cut-off can be the enabler for a FOD-free drill exit. However, dry machining increases temperature due to missing cooling and lubrication. Thereby, a higher thermal load is placed on the drill, possibly shortening tool life and risking overheating the CFRP matrix material.

This work focuses on developing a suitable exit strategy combined with optimizing the drill geometry while still fulfilling all quality requirements for the drilled hole. An overview of the different process stages proposed and investigated in this work is given in Fig. 2. Maintaining acceptable tool life despite the challenges described above is a prerequisite for the applicability of the added drill exit stage in industry.

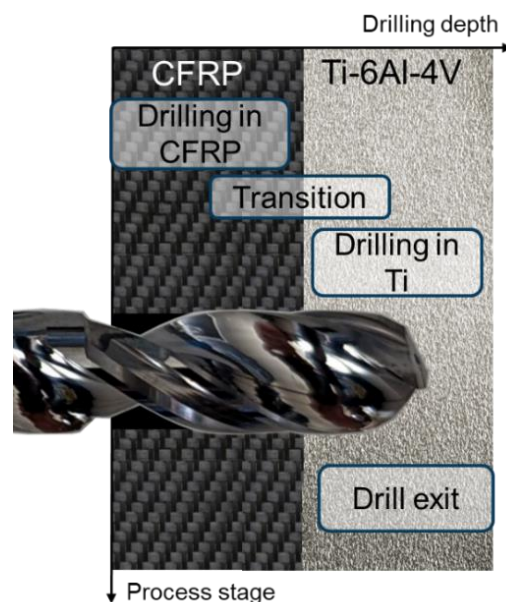


Fig. 2. Schematic overview of the drilling process stages

While previous research can improve the process speed and quality, foreign object debris (FOD) still remains an ongoing concern. To mitigate this, further advancements of the VAD process targeting the drill exit phase are presented in this study. The aim is to counteract FOD – in the case of this study chip particles – that are left behind in a closed structure.

2. METHODS AND MATERIALS

The experimental setup is shown in Fig. 3. A modified 4-axis CNC milling machine nb-h90 (Hüller Hille, Germany) forms the base for the experimental setup. The core component of the setup is the VAD drilling spindle. For this study, a LeviSpin (LTI Motion, Germany) is used. The spindle is equipped with electromagnetic bearings. Through the modulation of the bearing voltage, the spindle is able to move the rotor axially as well as radially. The axial oscillation can reach up to 300 Hz, a maximum amplitude of 120 μm is possible. Radial motion is not used for this investigation. Maximum rotational speed of the spindle is 12000 rpm [26].

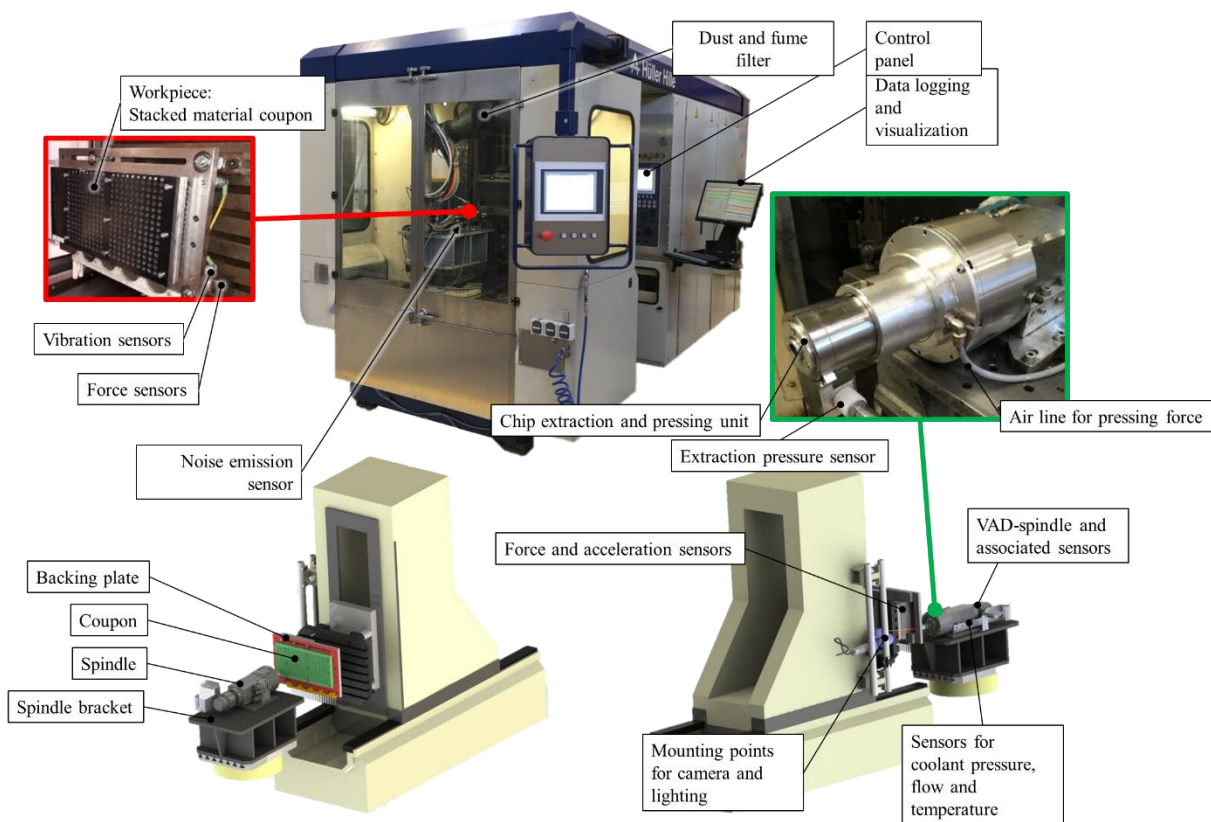


Fig. 3. Experimental setup on Hüller Hille nb-h90 machining centre

For chip extraction as well as providing a pressing force on the workpiece, a telescopic chip extraction cap specifically designed for the LTI spindle is mounted on the tip of the spindle. Using a compressed air feed, the telescopic part is pressed against the work piece. A pressure of 8 bar was used for all experiments, which correlates to approximately 1100 N of axial pressing force. Chip extraction is realized using an industrial vacuum machine 216 EX (Nederman, Sweden) that is connected to the extraction cap. The machine is set up for drilling experiments and is fitted with extensive sensor equipment. On the side of the work piece, four force sensors and four acceleration sensors are used. Next to the spindle, a noise

emission sensor is placed and coolant is monitored in regards of flow, temperature and pressure. Chip extraction can be monitored via a pressure (vacuum) sensor located near the tip of the chip extraction cap. All sensor data, including axis positions and spindle load data is collected and stored using a real-time embedded industrial controller, named compactRIO (National Instruments, USA), located inside electrical cabinet of the machine. A live data feed along with a graphical user interface is available on a monitor next to the control panel, where data logging can be controlled. An additional particle and fume filtration unit extracts air from the working area inside the machine and ensures a safe workplace environment. For lubrication, a Lubrix V7 (Lubrix, Germany) Minimum Quantity Lubrication (MQL) system is used, in conjunction with Boelube (Orelube, USA) as lubricant. The baseline MQL pressure is set to 8 bar. Compressed air is also available for cooling. Both MQL and compressed air are set up for internal cooling, routed through the spindle and drill. Via the CNC program, MQL or compressed air can be selected for each stage of the drilling process.

2.1. EVALUATION EQUIPMENT AND CRITERIA

For high speed videos, two systems were used based on their availability in the course of this study: A VW-9000E (Keyence, Japan) with a high-speed lens and a Motion Pro (Redlake, USA) camera system. The Keyence system is capable of capturing colour images with a frame rate up to 230000 fps and a maximum resolution of 1024×768 px, while the Redlake system records grayscale video with a frame rate up to 64 000 fps with a maximum resolution of 1280×1024 px. For this investigation, a frame rate of 3000 fps was used with both systems. With the exit speed of the drill of 750 rpm, one frame is recorded every 1.5° of rotation. This is sufficient for in-depth analysis of the chip formation and extraction. The setup in the machine is depicted in Fig. 4 using the Keyence system. The arrangement is the same when using the Redlake camera.

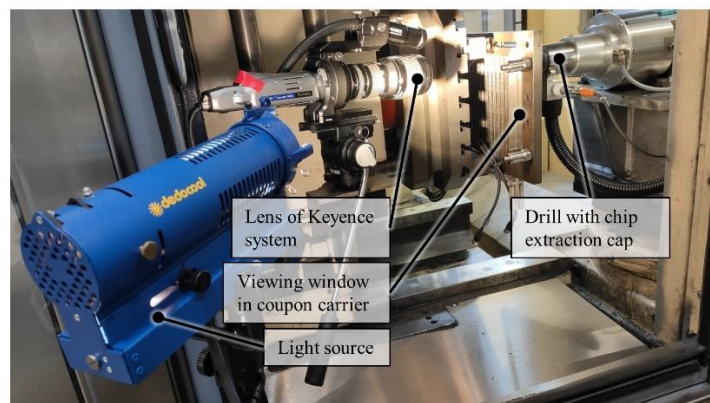


Fig. 4. Keyence camera system mounted in test bed

Thermal images were recorded using an Optris PI400 (Optris, Germany). The setup in the machine is depicted in Fig. 4. The drill was positioned 1 mm away from the coupon edge.

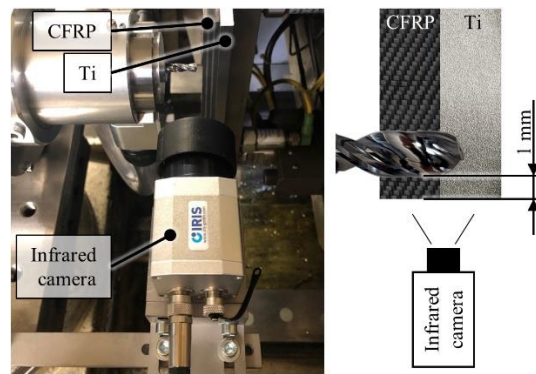


Fig. 5. Setup and schematic view of thermal camera

Tactile measurements were performed to evaluate key metrics of the boreholes. For both diameter and burr height, a MarCator 1087BR (Mahr, Germany) is used. This digital dial gauge with micron-resolution can be used in different configurations depending on the measurement task. In Fig. 6. left, the setup for diameter measurements is depicted, the setup for burr measurements is shown on the right side.

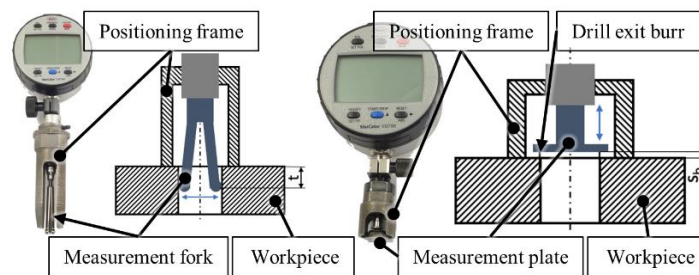


Fig. 6. Tactile measurement of diameter (left) and burr height (right)

Roughness measurements were performed using a MarSurf PS 10 (Mahr, Germany). The measurement setup is shown in Fig. 7. It consists of a scissor table for precise alignment of the stylus and drive unit, a separate hand device and digital connection for data logging. Since the evaluation criteria is solely based on R_a values, this metric is of prime interest. The surface roughness was evaluated according to the ISO 4288 standard.

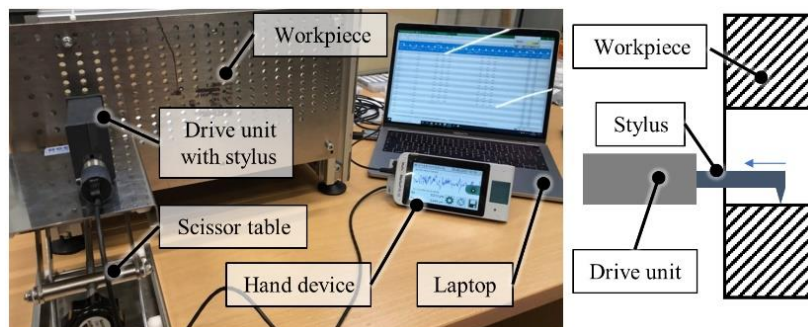


Fig. 7. Measurement setup for borehole wall roughness

In order to determine whether a borehole is acceptable, quality criteria are needed. These are provided by plane manufacturer's internal guidelines. For the hole in Ti, 5 criteria must be met: diameter, diameter spread, entry burr height, exit burr height, and wall roughness. Figure 8 shows the acceptable values for each quality criterion. For CFRP, the tolerances regarding the diameter and diameter spread are the same, but instead of burr height, there must be no visible delamination. Roughness measurements are omitted on the CFRP layer.

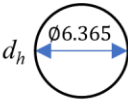
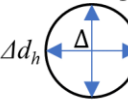
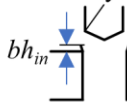
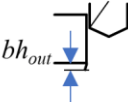
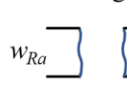
Quality criteria	Diameter	Diameter spread	Entry burr	Exit burr	Wall roughness
Symbol					
Tolerance	6.315...6.395 mm	< 0.045 mm	< 0.125 mm	< 0.200 mm	Ra < 1.6 μm

Fig. 8. Quantitative quality criteria for the drilled holes

2.2. MATERIAL COUPONS

In this study, a material stack consisting of an outer layer of CFRP (drill entry) and an inner layer of Ti-6Al-4V (drill exit) is investigated (compare to Fig. 2). The material is present as flat sheet coupons with dimensions of 400 mm x 200 mm. The arrangement of the coupons can be seen in Fig. 9 alongside a comparison to a typical application for this stack material.

The thickness of the CFRP layer is 10 mm. The material is certified for aerospace applications, and the fibre orientations correspond to proprietary OEM specifications. It consists of a quasi-isotropic UD-layup in an epoxy matrix. Fibre orientation is 0°, 90° 45°, and 135°. Each fibre orientation makes up 25% of the material thickness. The top layer is made of GFRP in order to reduce fraying and delamination defects. The titanium material is also sourced from a certified manufacturer, with a thickness of 8.5 mm. Its mechanical properties are given in Table 1. The total stack thickness amounts to 18.5 mm. Stack material in this exact configuration is used for manufacturing wing structures for commercial airplanes.

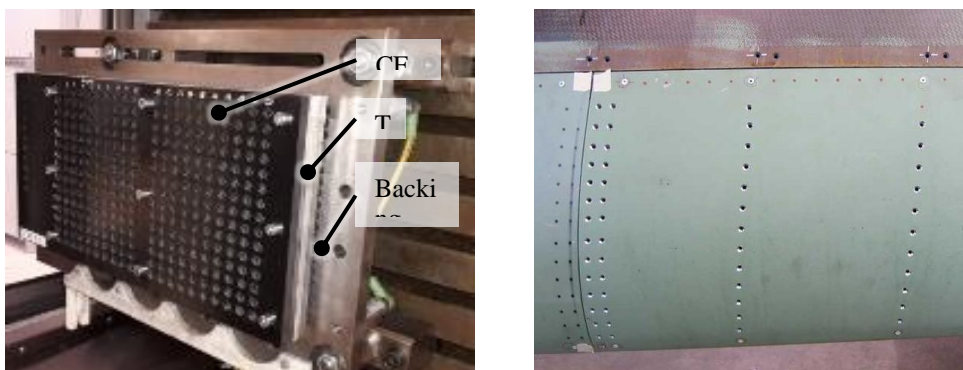


Fig. 9. Material stack on mounting plate (left) and comparison to actual component (leading edge of wing) [27] (right)

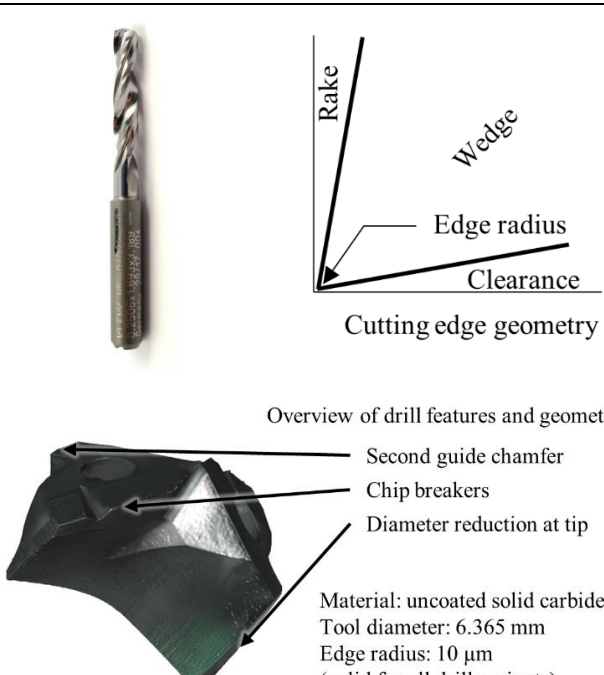
Table 1. Material properties of the used material Ti-6Al-4V

Alloy	Ti-6Al-4V
Material number	3.7164
State	solution-annealed
Yield strength $R_{p0.2}$	830 MPa
Tensile strength R_m	895 MPa
Elongation at break A	10%
Density ρ	4.43 g/cm ³
Young's modulus E	114 GPa
Thermal conductivity α	7.1 W/mK
Hardness HB	310

2.3. DRILLING TOOLS

An integral part of this study is the investigation of different drill geometries to develop the drilling process in the specified stack material. For this, a baseline drill geometry, designated as v0, is used as the starting point. The tool is specified for drilling of landing flaps and it is made of uncoated solid carbide. The main characteristics of the drilling tool are listed below in Table 2.

Table 2. Specifications of baseline drill type

Baseline drill (v0)		
Vendor	Klenk (Germany)	
Type	HB-04923-02	
Tool material	WC-6Co	
Coating	none	
Diameter d_B	6.365 mm	
Cutting length	43 mm	
Point angle σ	135°	
Twist angle δ	30°	
Rake angle γ (outside/inside)	10°/7°	
Wedge angle β (outside/inside)	69°/72°	
Clearance angle α (outside/inside)	11°/11°	
Number of guide chamfers	4	
Offset second guide chamfer	65°	
Chip breaker	Yes	
Lubricant hole \varnothing	1 mm	

From there, specific features of the drill bit were removed or altered by regrinding. In Fig. 10 an overview of the tested drill geometries is given. All drills have a diameter of 6.365 mm (approx. 1/4 in). This type of diameter is very common for rivet drills in wing

structures [27]. Cutting edge radius measurements were performed in house using optical systems (Alicona, Austria) with a result of $10 \pm 1.5 \mu\text{m}$ for all investigated drill variants. All drilling tools used can be operated with MQL through existing lubricant holes. As a result, the lubricant can be introduced directly into the cutting area.

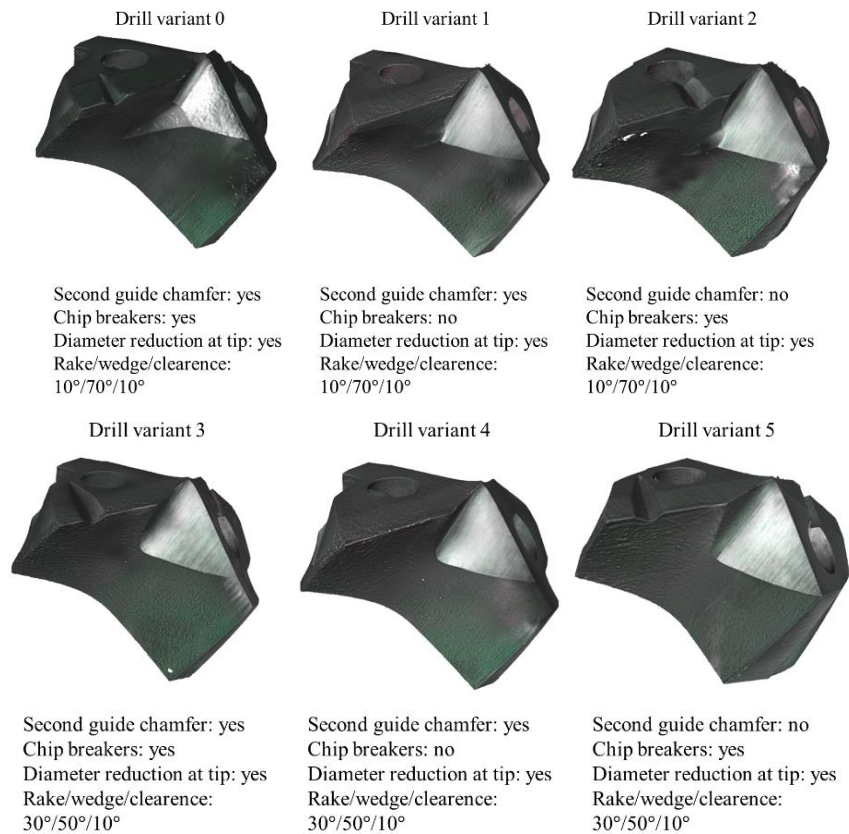


Fig. 10. Investigated drill variants

All drill variants are equipped with a side chamfer in the cutting edge corner area. This reduces the effective diameter in this area to 6.35 mm. In principle, the use of conventional drills without a side chamfer can cause ring burrs with/without drill caps as well as crown burrs, which depend on the respective geometry and parameter set. The length of this chamfer is 1.6 mm. This must be taken into account in the feed path after drill exit to ensure the nominal diameter is reached. The engagement via the guide chamfer and the resulting peeling process to the full diameter ultimately results in a lower burr height [28].

2.4. FOD-FREE MANUFACTURING AND PROCESS DEVELOPMENT

One important aspect in enhancing the complete manufacturing process for drilling rivet holes is FOD-free manufacturing. FOD-free is a common term in aerospace, generally meaning to leave no artefacts behind. This ranges from hand tools found behind cabin panels

to burrs breaking loose and being trapped in a part [29]. When drilling rivet holes – regardless if the quality criteria of the drilled hole is met – there is usually accumulation of chips, cutting fluids or remains of lubricants which remain in the drill hole or stuck to the surface. Especially when drilling enclosed structures like flaps and wing boxes, this usually necessitates disassembly, deburring, cleaning, and reassembly. One key problem when drilling enclosed structures is the cap and the burr formation on the exit side of the drill. Cap and burr formation in drilling are linked and it is primarily dependent upon the tool geometry and the orientation of the cutting edge to the exit surface of the hole [30].

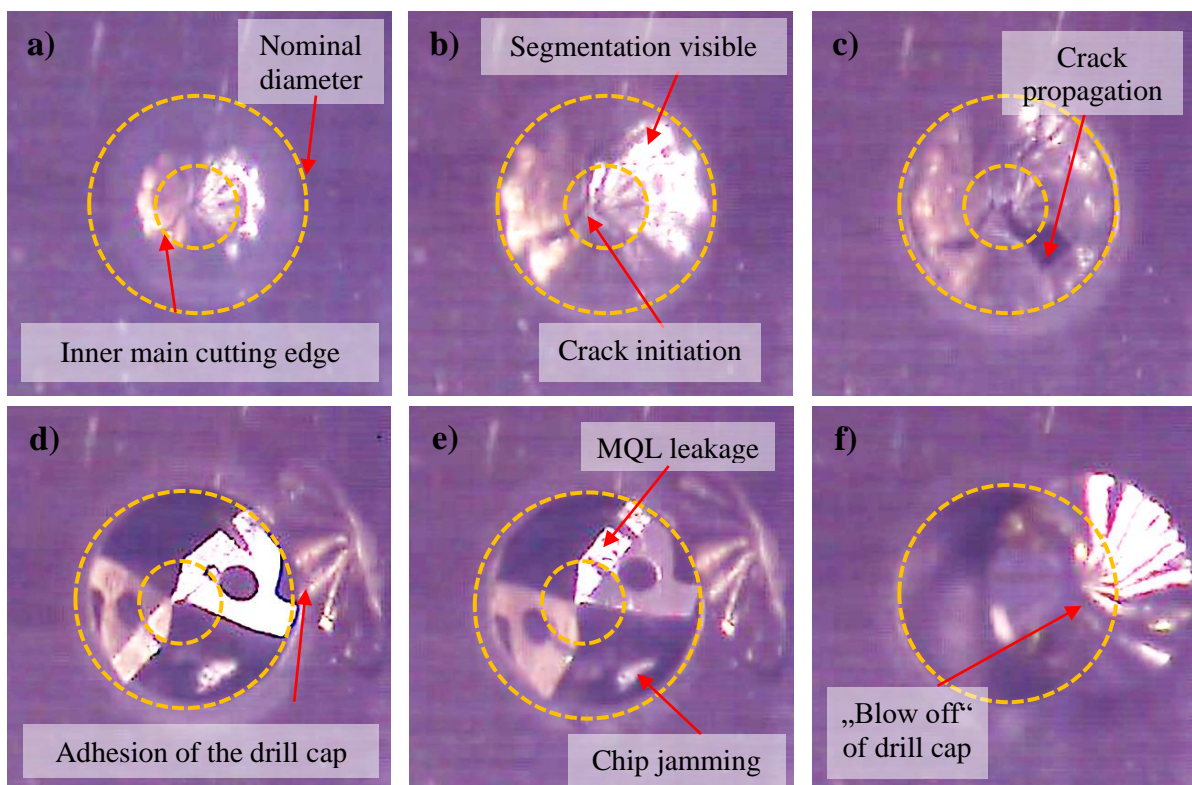


Fig. 11. Drill cap formation in Ti-6Al-4V Tool: v0 with exit parameter 1 ($v_c = 15$ m/min, $f = 0.2$ mm, $A = 0.08$ mm, $F_s = 12$, no dwell time)

During the process of forming the drill cap, raised material known as a burr is generated. These burrs can be classified into four distinct categories [31]. The ideal outcome is the production of a small, uniform burr, that falls within the required tolerance and requires no additional processing. Conversely, uniform burrs with torn drill caps, crown burrs and uniform burrs with petals are all undesirable outcomes that result in elevated rework costs. To meet the quality criteria of a drilled hole, all chips and caps must be able to be removed by vacuuming during the entire drilling process, including the exit of the drill bit. Burrs and therefore caps are formed by a sequence of events that begin when the drill deforms the material on the exit surface of the workpiece. The process of drill cap formation in Ti-6Al-4V can be seen in Fig. 11.

The process used to exit the titanium material is vibration assisted machining. In this specific case, VAD is not actively used for chip breaking. A more detailed description of the VAD process and its parameters is given in section 0. Although an exact segmentation according to the specific frequency of the axial tool oscillation can be seen (Fig. 11b), no material is cut out of the forming drill cap. Only cracking occurs on the drill cap (Fig. 11b-c). The drill cap gets pushed out and remains connected to the material via the ridge. The burr formation starts by exceeding the permissible local mechanical stress of the material in the cutting zone. The workpiece begins to deform plastically and this results in high compressive stresses on the material if the feed force remains constant. Burr and drill cap formation usually occurs due to initial cracking at the centre of the hole, where the cutting edge exerts high compressive stresses on the material (Fig. 11b-c). At a constant drilling feed rate, the area of plastic deformation increases from the centre to the outer edge of the drill, and a second crack formation occurs in the area of the outer cutting corner. This results in the formation of a drill cap. It is also common, that the drill cap does not become fully detached from the material, but remains stuck on a small portion of the perimeter (Fig. 11d-f).

In order to meet the requirements of FOD-free drilling, a suitable configuration of drill geometry, process parameters and chip extraction must be found to ensure compliance with the required quality criteria on the one hand and residue-free drilling on the other. With a full FOD-free drilling process, including no contamination of chips and cutting fluids, which also meets all quality criteria mentioned above, the manual disassembly and post-processing can be omitted. This is usually referred to as one-up-assembly [14], where a structure is only built up once. A FOD-free process can be seen as the enabler for one-up-assembly, which in turn can generate substantial efficiency gains. Savings up to 50% in lead time for each single drilling cycle are feasible, based on omitting of de- and re-assembly steps [32]. The main barrier for FOD-free drilling can be seen in the drill cap formation and the chip evacuation. To overcome the mechanism of drill cap formation and positively influence the chip segmentation, the implementation of low frequency VAD is used to generate controlled chip breaking by superimposing a cyclic vibration on the axial feed motion of the tool. By modulating the frequency and amplitude of the VAD process, the cutting conditions can be altered, leading to the creation of a diverse array of chip shapes. To supplement and validate the empirical investigation, a kinematic simulation of the VAD process was generated using a conventional programming language. The computational model employed in this study characterizes the drilling process of a tool possessing two cutting edges and permits the computation of the (non-deformed) chip shape as a function of the main process parameters. Figure 12a illustrates the outcomes of a conventional drilling kinematic utilizing a two-cutting edge tool, with an unchanging uncut chip thickness. This results in a continuous chip formation that is challenging to remove and heightens the potential for damage to the CFRP material due to its geometry. Conversely, Fig. 12b showcases the zone of engagement of an intermittent tool/workpiece interaction produced by the axial oscillation of the tool. The region of intersection between the actual workpiece surface and the tool generates a varying uncut chip thickness when the VAD technique is employed. Relevant process parameters are cutting speed v_c , feed per tooth f_z , amplitude A and frequency F . The specific frequency ratio F is defined as the ratio between the frequency of the axial vibration f_a and the rotational frequency of the tool. The linear feed movement, which is determined by the

feed per revolution, is overlaid with a sinusoidal oscillation determined by the axial amplitude and specific frequency ratio. The combination of these movements yields the complete path of the tool. Based on the model, predictions can be made as to whether a discontinuous cut can be achieved by the intended process setting. In the case of a discontinuous cut, the tool is not permanently engaged, which forces chip breakage and, by facilitating chip removal of the smaller chip segments, an improvement of the process can be achieved even without retraction of the tool.

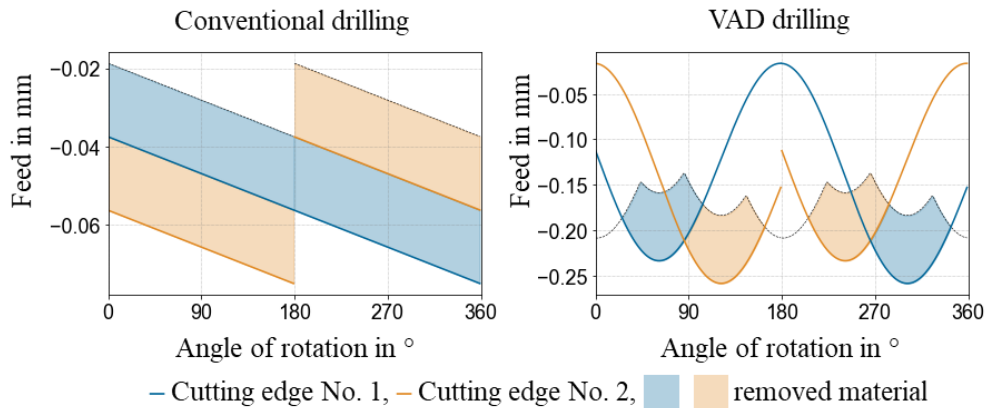


Fig. 12. Kinematic tool/workpiece interaction in a) conventional drilling and b) discontinuous tool/workpiece interaction using VAD

In the subsequent stage, the process necessitates adaptation to determine a methodology for drill cap destruction in the titanium layer. If a specific frequency F is employed for the main hole that is not an integer multiple of the number of cutting edges (i.e., 1.5 and 2.65), the rotational frequency for drill cap destruction is intentionally selected as an integer multiple of the number of cutting edges. This generates segments on the drill cap that are periodically “peeled off” by the main cutting edges in the ideal circumstance. However, it is anticipated that continuous chip formation will commence prior to the peeling process of the drill cap by the two cutting edges since the exit parameter is switched to 0.5 mm before the drill exits the material.

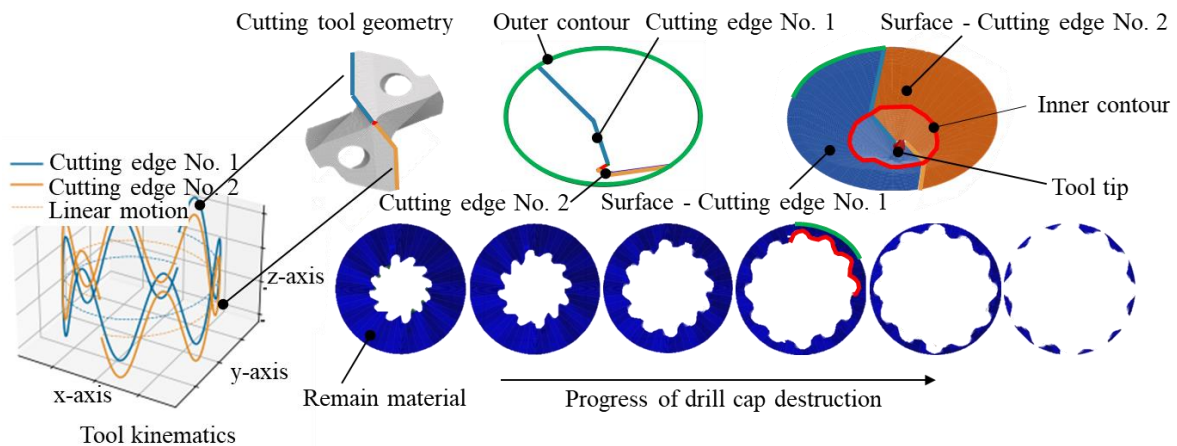


Fig. 13. Tool kinematic simulation using VAD for drill cap destruction and its generated borehole surface

The process kinematics for drill cap destruction in the titanium layer is illustrated in Fig. 13. The left-hand side depicts the progression of the cutting edge corners 1 and 2 over the lateral surface of the bore wall for a superposed feed progression. As observed, there is no overlap of the trajectories of both cutting corners for the specified parameter set, resulting in the long chip discussed earlier. Utilizing this tool kinematics and the macro-geometry of a drill bit, a three-dimensional simulation of the chip formation with a two-cutting-edge tool can be conducted. Each cutting edge comprises three sections: The chisel tip, inner main cutting edge, and outer main cutting edge, and its geometry is completed by specifying the tip angle σ and the diameter of the drill d . Since this simulation represents an idealized cutting process, rake, wedge, and clearance angles are not necessary since the cutting edge is assumed to be perfectly sharp. The input parameters are completed by specifying the total material thickness. During the simulation, the program algorithm advances the tool by half a rotation, checks the positions at which material was removed, and generates an image of the current bottom surface of the bore hole. At any given time, both cutting edges remove the same amount of material. Hence, calculating the tool movement in steps of one full revolution would be sufficient. However, by advancing in 180° steps, the full drilling progress is plotted, allowing complete monitoring of the drilling process. The kinematic model is employed to assess various frequency and amplitude ratios before the experimental investigation and to verify the process influences after the investigation (see section 3.2).

2.5. DESIGN OF EXPERIMENT

For the main borehole in Ti, a non-integer specific frequency ratio of 2.65 was used for effective chip breaking. This is based on the kinematic model as well as on previous investigations at the institute [33]. For the exit strategy, specific frequency ratios have to be used as even integers as mentioned in section 2.4. Higher specific frequency ratios are assumed to be more effective, since more material is removed per revolution. Therefore, all drill geometries were tested at $F = 12$ for the first investigation. After evaluation of the first test series, the best grill geometry was benchmarked against the baseline geometry at lower specific frequency ratios ($F = 6, 8, 10$) to conform the assumed thesis. The full set of drilling parameters for CFRP and Ti (see Fig. 2) is given in Table 3. The parameters for CFRP and Ti (excluding the exit) are already optimized parameters based on previous tests which are not part of this work, and are therefore fixed for this investigation.

In Fig. 14, an example process is shown using the main parameters v_c, f, A , and F , from which the other parameters in Table 3 are calculated. The first section in CFRP is drilled using a higher cutting speed and feed, but without oscillation; hence A and F are zero. At 0.5 mm before the drill tip reaches the layer boundary, the parameters are switched to the Ti parameter set. Here, oscillation is used with $F = 2.65$, and $A > f$ in order to move out of the cut and kinematically break the chip. The layer transition is completed when the corners of the cutting edges are in full contact with Ti. Within the transition phase, mixed chips of CFRP and Ti are produced. The second transition starts 0.5 mm before the drill tip exits the material. Here the process is switched to the exit parameter set. This example shows Ti exit 1 with $F = 12$. Here, $A < f$ is used to ensure a sustained removal of chips during the machining process. Since all

drills have a diameter reduction of about 3% at the tip, the drill feed is continued by another 3 mm to ensure that the nominal diameter is reached.

Table 3. Investigated process parameter set

Phase	CFRP	Ti	Ti exit 1	Ti exit 2	Ti exit 3	Ti exit 4
Spindle speed, n in rpm	6000	750	750	750	750	750
Cutting speed, v_c in m/min	120	15	15	15	15	15
Feed, f in mm/rev	0.14	0.075	0.2	0.2	0.2	0.2
Feed rate, v_f in mm/min	840	56	150	150	150	150
Axial amplitude of oscillation, A in mm	0	0.12	0.08	0.08	0.08	0.08
Specific frequency ratio, F	0	2.65	12	10	8	6
Axial oscillation frequency, f_a in Hz	0	33	150	125	100	75
Cooling	MQL	MQL	Air	Air	Air	Air

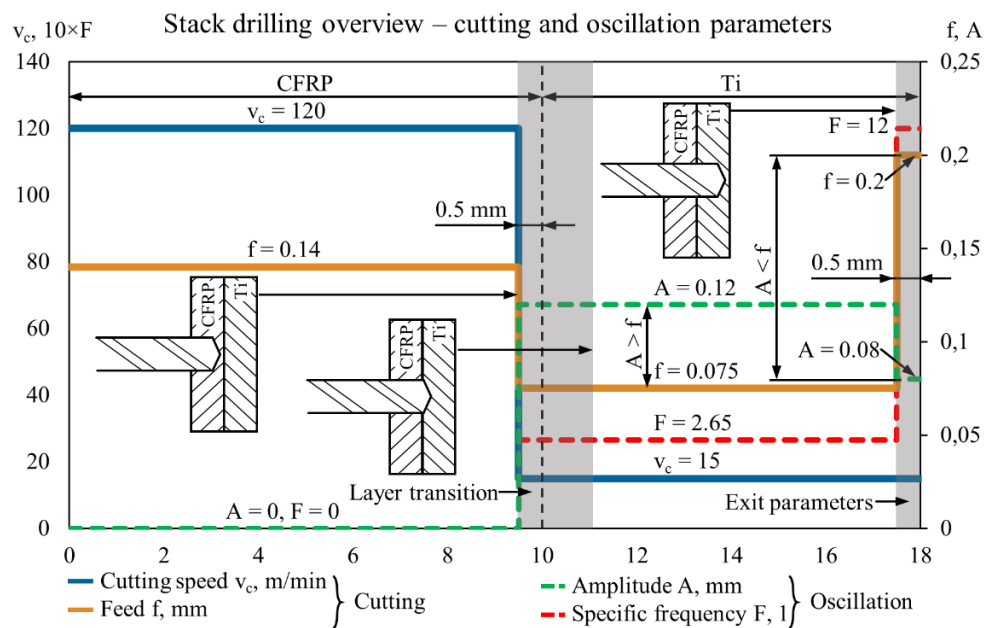


Fig. 14. Example process showing parameter sequence CFRP – Ti – Ti exit 1

3. EXPERIMENTAL INVESTIGATION

3.1. INVESTIGATION OF DIFFERENT DRILL BIT GEOMETRIES

A preliminary investigation for all drill geometries was performed at $F = 12$ in order to determine the most suitable drill geometry. Since the majority of the work is drill cap

destruction, this first investigation is performed in Ti only. The best performing drill geometry is then benchmarked in-depth against the baseline variant 0 in a CFRP-Ti stack.

Borehole quality is the most important aspect in terms of part quality, so this metric is evaluated first. The results for all drill geometries at $F = 12$ are given in Fig. 15. For comparison, the results of geometry v0 are also given when using conventional drilling ($F = 0$) in the last column. The acceptable range of the diameter is illustrated by the limits of the scale (6.315...6.395 mm), while the desired diameter of 6.365 mm is indicated with a dashed line. The threshold value for the remaining quality metrics is presented in the top right corner of the graph, with a dashed line displayed if the threshold is within the scale of the graph. All modified variants conform to the quality requirements, except for the baseline v0 which fails to produce satisfactory exit burr heights and roughness values using the utilized parameter set (Ti - Ti Exit 1, as presented in Table 3. It should be mentioned, that the drills featuring sharper cutting edge angles (v3-v5) generate substantially smaller burrs on both entry and exit. These drills exhibit a greater diameter spread, yet even the worst-performing drill in this regard is still 5.6 times lower than the threshold of 0.045 mm.

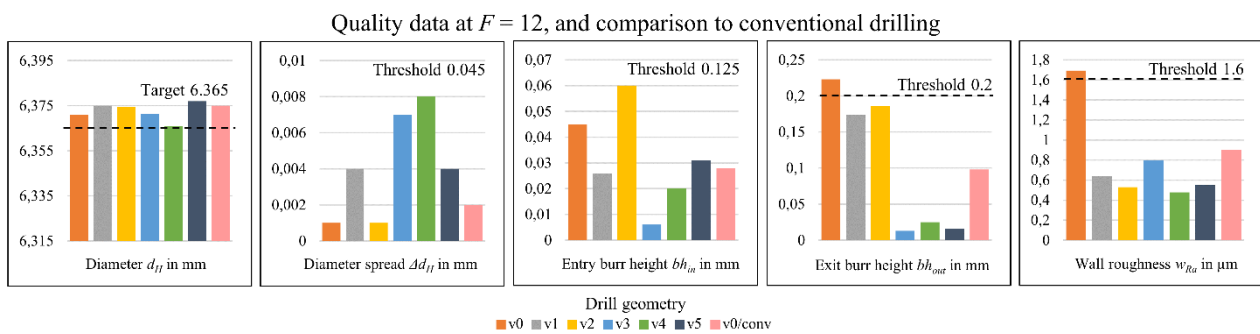


Fig. 15. Quality data for first investigation

A simple unweighted score S is introduced in Eqn. (1) in order to objectively evaluate the quality data. The metric used to evaluate the quality of the borehole is a score, where a higher value indicates better quality.

$$S = (|6.365 - d_H| \cdot \Delta d_H \cdot bh_{in} \cdot bh_{out} \cdot w_{Ra} \cdot 10^6)^{-1} \tag{1}$$

The results are given in Table 4 below. At $F = 12$, geometry v4 is best suited, followed by v3, v5, v2, v1 and baseline v0. It is noteworthy that baseline v0 performs better with the intended conventional process for this application. For comparison, a result on the threshold of every quality metric (i.e. the worst still acceptable hole) would yield a score of 0.011.

Table 4. Drill score for each tested drill geometry

Drill variant	v0	v1	v2	v3	v4	v5	v0/conv
Score S	9.82	8.66	17.80	354.87	525.21	76.37	20.18

The high-speed video of the drill exit and drill cap destruction show similar results regarding the suitability of the drill geometries (Fig. 16). Drills v0 and v2 exhibit a full-size

drill cap which is prone to crack formation at the perimeter. In the case of drill v1, it produces noticeable crown burrs, and while the resulting drill cap is smaller, it is still too large to be extracted through the drill flutes. The same is applicable to drills v3 and v5, despite smaller exit burrs. The diameter of the drill cap produced by the drills with chip breakers is dependent on the position of the inner chip breaker. Hence, drills without chip breakers are preferred for drill cap destruction. Only the drill geometry of v4 yields a sufficiently small drill cap that can be extracted effectively. A summary of the drill geometries and their suitability for drill cap destruction is given in Table 5.

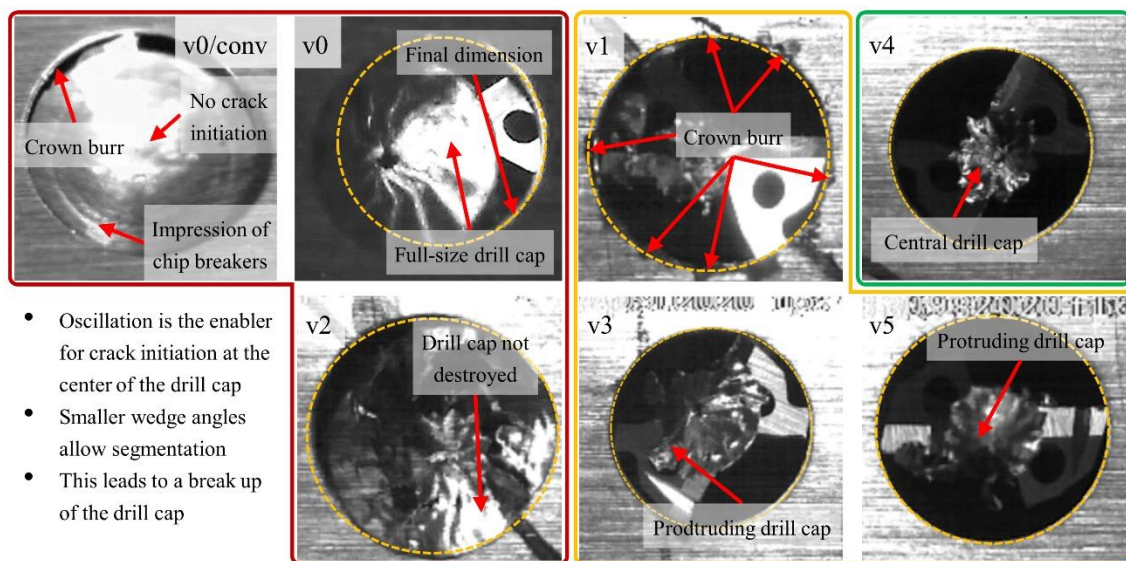


Fig. 16. Drill exit and drill cap destruction for all investigated geometries

Table 5. Suitability of drill variants for drill cap destruction

Drill variant	Rake/Wedge/Clearance	Chip breakers	Second guide chamfer	Diameter reduction at tip	Suitable
0	10°/70°/10°	Yes	Yes	Yes	No
1	10°/70°/10°	No	Yes	Yes	Partially
2	10°/70°/10°	Yes	No	Yes	No
3	30°/50°/10°	Yes	Yes	Yes	Partially
4	30°/50°/10°	No	Yes	Yes	Yes
5	30°/50°/10°	Yes	No	Yes	Partially

For this work, the main focus lies on developing a suitable strategy for drill cap destruction. This is why the mainly investigated aspects are the high-speed images and the reached borehole quality. However, the process force is also evaluated for this study in order to see how the axial force correlates to the drill geometry and process alterations. The process force is a superposition of the feed force and the pressing force of the chip extraction cap. An overview of such a position-process force plot for a CFRP-Ti stack is depicted in Fig. 17. The first phase is the approach of the spindle unit. When the chip extraction cap comes into contact with the workpiece surface, the pressing force of about 1100 N is registered. Next, the drill comes into contact with the outer CFRP layer and feed force rises accordingly.

A stable force level is reached when the cutting edges are in full contact with the workpiece. The switch to the parameter set for Ti is done 0.5 mm before the layer transition and is accompanied by a short retract of the spindle, which can be seen as force drop in the graph. Spindle oscillation is also activated at this stage. Hence, the smoothed force also shows a fluctuation of the force magnitude. Another parameter switch occurs 0.5 mm before the drill exit. Here, feed f and frequency f_a are increased, resulting in a higher feed force, which gradually decreases while the tip of the drill is exiting the material. Due to the diameter reduction at the tip, feed is continued for 3 mm more in order to ensure the nominal diameter is reached. In the remaining graphs, a cropped in view is shown.

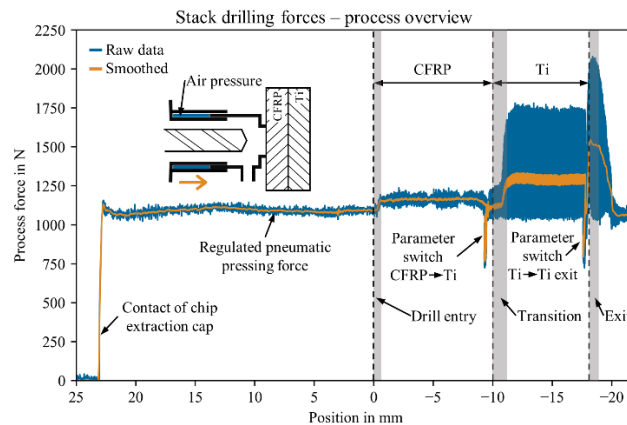


Fig. 17. Example position – process force graph

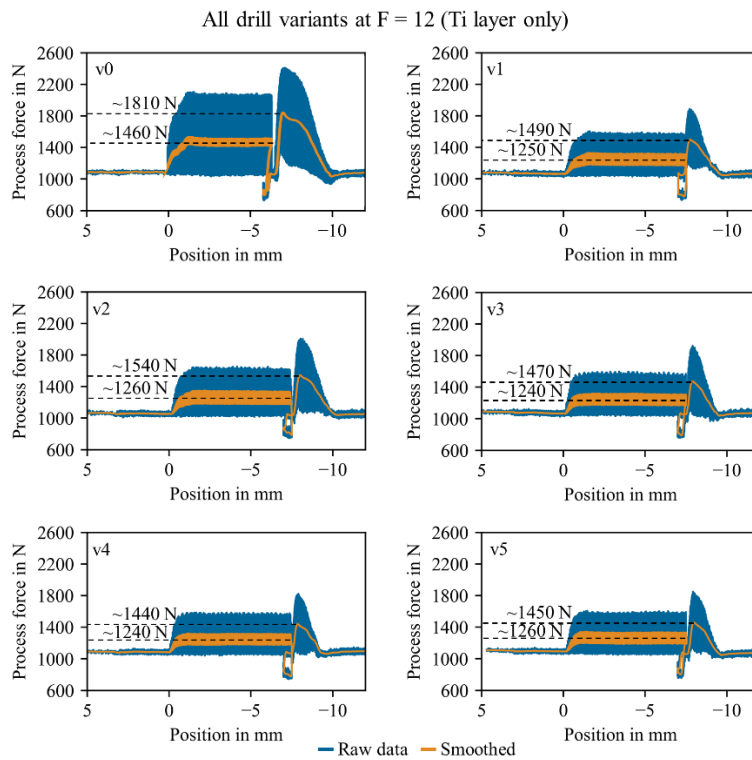


Fig. 18. Position-force plots for all investigated drill geometries at $F = 12$

Figure 18 shows the process forces for all drill geometries. Since this test is only done in the Ti layer, only the sections regarding the Ti and exit are present. Two force levels are annotated on each graph: A graphical average of the smoothed process force for the Ti parameter, and the maximum of the smoothed force for the drill exit. While drills with lower forces tend to produce better quality metrics, no clear correlation can be found. However, it is assumed that a lower force means less tool wear, resulting in increased tool life.

To summarize this section, it is clear that drill geometry v4 is most suitable. The quality score is 48% higher than the second-best geometry v3, and higher by over 530% compared to the baseline v0. Variant 4 is the only drill geometry able to break the drill cap sufficiently for extraction and also produces the lowest process forces, indicating a cleaner cut and higher tool life.

3.2. IN-DEPTH ANALYSIS FOR BEST DRILL BIT GEOMETRY

This section aims to compare the performance of the promising variant v4 with the baseline drill geometry v0. Drilling experiments are conducted in CFRP-Ti stacks to ensure experimental conditions close to the actual manufacturing process. Here, four different exit parameters are investigated, differing in the specific frequency F (Ti Exit 1–4, compare to Table 3) in order to test the hypotheses that higher F yields better results. In Fig. 19, the quality data is given. Table 6 shows the score S according to Eqn. (1).

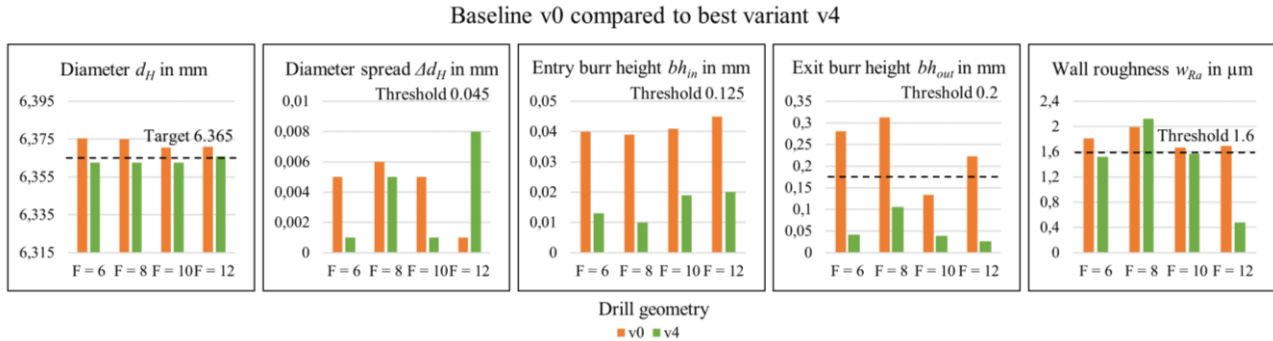


Fig. 19. Compared to the baseline v0, geometry v4 is especially advantageous at higher specific frequency ratios

Table 6. In-depth analysis and drill score comparison of drill type v0 and type v4

Parameter	$F = 6$		$F = 8$		$F = 10$		$F = 12$	
Drill variant	v0	v4	v0	v4	v0	v4	v0	v4
Score S	0.93	505.08	0.69	36.16	3.97	363.80	9.82	525.21

It is clear to see that geometry v4 consistently produces better results. Geometry v0 is not able to produce satisfactory exit burr heights in most and wall roughness in all cases. Considering the quality score, the hypothesis of beneficial higher frequencies is partially confirmed. $F = 12$ shows the highest score for both drills. $F = 10$ also shows high score values, especially for drill v0. At $F = 8$, both drills have the worst performance. Due to the low diameter spread and exit burr height, drill v4 has its second to highest score at $F = 6$.

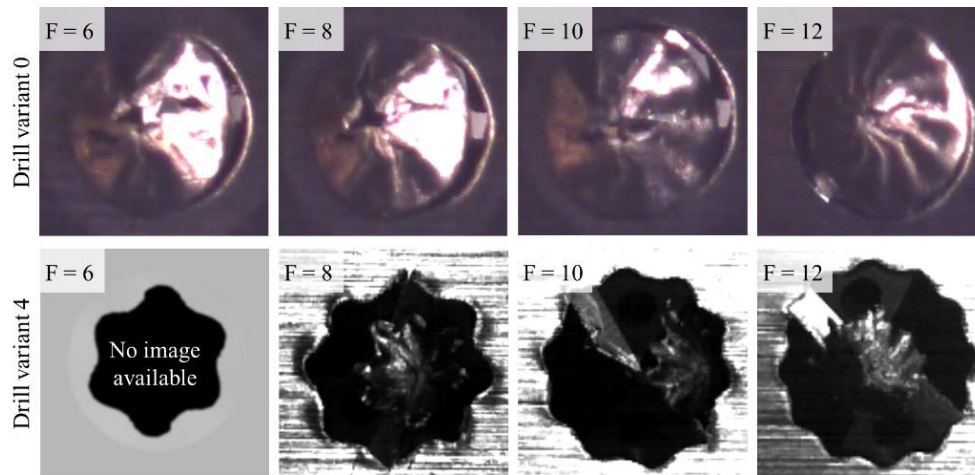


Fig. 20. Drill cap destruction at different specific frequencies

The results regarding the drill cap destruction are shown in Fig. 20. The reference drill v0, depicted in the top line, consistently generates a full-size drill cap regardless of the process parameters. The waviness caused by the different specific frequencies is clearly visible. Drill v4 (bottom line) is capable of drill cap destruction at all shown parameters. It has to be noted that due to corrupted data no images of the drill exit at $F = 6$ are available for this drill. With drill v4, a distinctive pattern at the outer edge of the borehole is visible. The number of lobes correlates to the specific frequency. Since F is an even integer, a regular pattern is formed. Due to the sharper cutting edge and the removed chip breakers, material is removed rather than deformed, leaving behind a much smaller central drill cap which can be extracted through the flutes of the drill. While a satisfactory result is reached at lower F , the smallest drill cap is formed at $F = 12$.

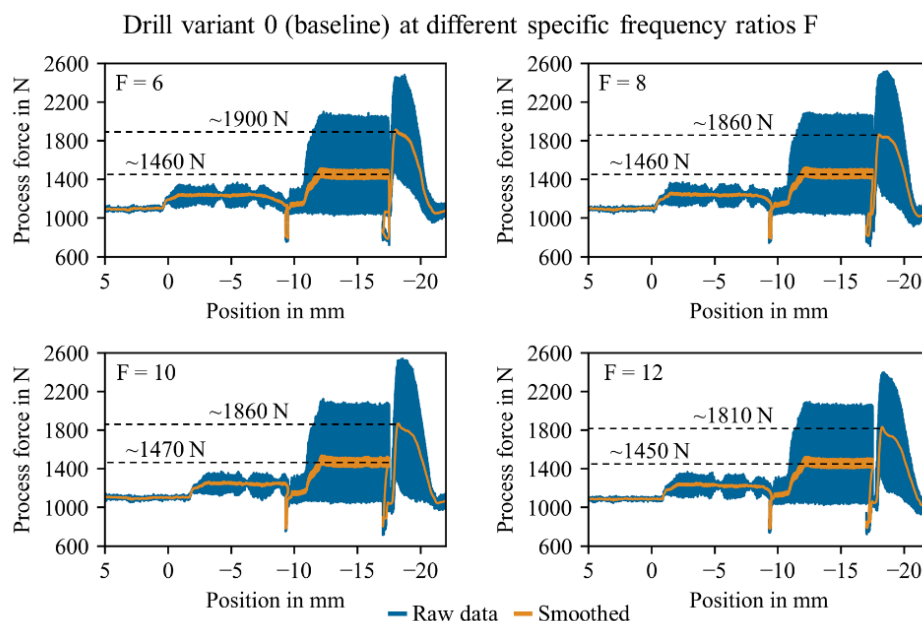


Fig. 21. Process force for drill variant 0

Process forces are shown in Figs 21 and Fig. 22. A decrease in mean and maximum force (dotted lines) can be noted with rising F , drill variant 4 also shows smaller process forces in the range of 10% for all investigated parameter sets. This further supports the proposed shift towards higher specific frequencies as well as the suitability of the modified drill geometry, again indicating a longer tool life.

As a final aspect, a thermal analysis shows the difference in temperature between conventional drilling and vibration assisted drilling (Fig. 23), and the exit parameter 1 with no exit parameter (Fig. 24). The temperature near the drill tip and at the layer interface CFRP-Ti are investigated. The aim is to understand the impact of VAD on the drill temperature and the layer interface, in order to ensure no overheating of the CFRP matrix takes place. It has to be emphasised, that the temperatures are recorded on the edge of the workpiece according to Fig. 5, so especially the temperature of the drill can only be seen as a rough reference. In Fig. 23, three different drill depths are compared. The parameter set is CFRP-Ti (no exit parameter), with drill variant 0. As expected, the interface temperature is highest when the drill is shortly after the transition, while the temperature of the drill rises with the drilling progress in Ti. No critical temperature levels were recorded. Since the process forces are highest with this drill geometry, it can be assumed that temperatures are even lower when using the modified drill variants.

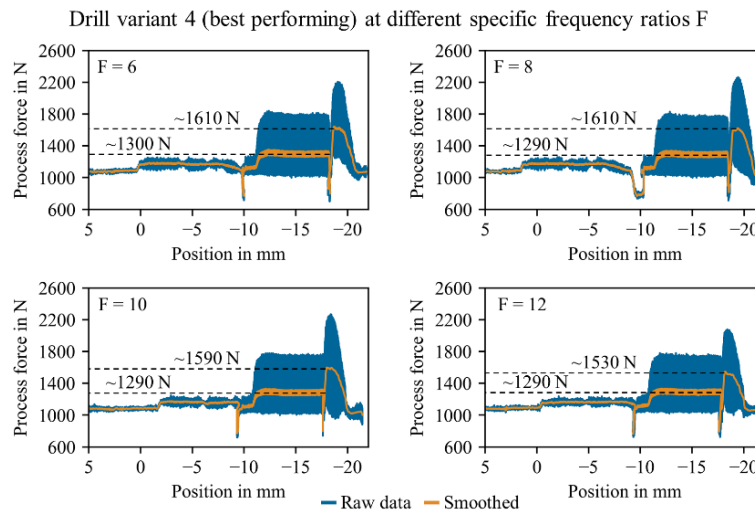


Fig. 22. Process force for drill variant 4

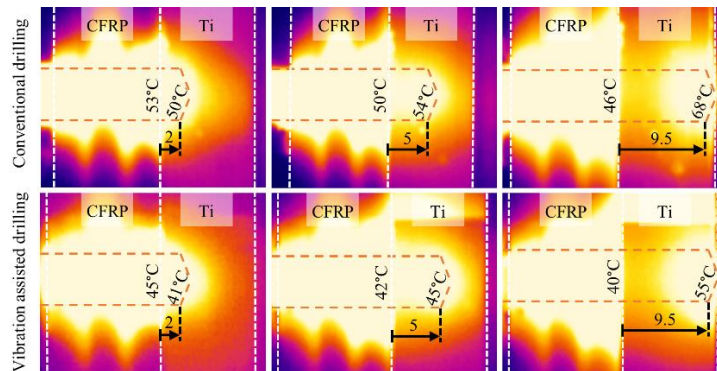


Fig. 23. Comparison of interface and tip temperature

In Fig. 24, the drill exit between parameter Ti (left) and Ti exit 1 (right) are compared using drill variant 0. Since the exit parameters use no oil lubrication, the drill temperature rises significantly in this process phase. However, due to the low thermal conductivity of 7.1 W/mK for Ti, this increase in temperature is not transmitted to the layer interface. Therefore, the use of a dry drilling exit parameter remains uncritical for the CFRP layer.

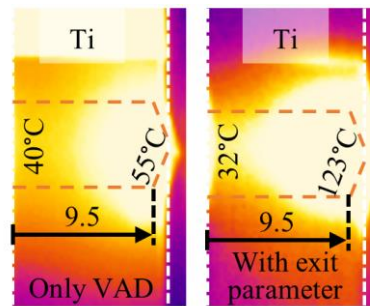


Fig. 24. Comparison of exit temperature when using VAD (left) and special exit parameter (dry drilling) (right)

3.3. SUMMARY

Borehole quality is most influenced by cutting edge angles and chip breakers. A sharper cutting edge is especially advantageous for reducing exit burr heights. The drills with a rake angle of 30° and a wedge angle of 50° yield a tenfold decrease in exit burr height compared to the drills with rake angle 10° and wedge angle 70° . Comparing drills with the same cutting edge angles, removal of the second guide chamfer resulted in a larger diameter error (v0 compared to v2, v3 compared to v5). The reason for this is a lack of radial support of the drill in the borehole, resulting in higher eccentricity and thereby enlarging the borehole diameter. Removal of the chip breakers has no clear influence on the borehole quality. From the data available, it seems that average roughness R_a is slightly improved. However, a drill without chip breakers performs significantly better in the drill cap destruction. A key factor of the exit strategy is removing the drill cap as continuous chips. This equivalent to suppressing chip breaking during the drill exit. It is clear that chip breakers are counterproductive for this. Since there is the possibility to kinematically break the chip when using vibration assisted drilling, a drill without chip breakers can be used without any disadvantage. When comparing the process forces for drill v0 and v4, the adapted geometry shows smaller values at all stages of the drilling process, mainly due to the increased sharpness of the cutting edge. Process forces show a tendency to decrease at higher F , indicating higher tool life when using these parameter sets.

4. CONCLUSION AND OUTLOOK

In this work, a method to avoid drill cap formation in Ti using vibration assisted drilling with defined coupling of the axial oscillation to the rotational frequency is introduced. A combination of several process-improving technologies/strategies could be shown in the laboratory environment. The intended use of this method is rivet hole drilling, which is a core

competence in aircraft construction. Current processes used show enormous potential for efficiency increase by reducing the mainly manual post-processing of the drilled parts by deburring and cleaning. The main findings of this work are:

- Vibration assisted drilling can be the key element for cap destruction.
- The geometry of the drill has an influence on the destruction of the drill cap.
- Sharper cutting edges are better suited for cap destruction.
- Chip breakers are counterproductive for cap destruction.
- Process parameters and drill geometry must be tuned together.
- Higher specific frequencies are more suitable for drill cap destruction.
- The results from the kinematic simulation confirms the process results for cap destruction and thus supports a high process reliability.
- The process sets very tight limits with regard to the parameter space.
- Thermal analysis shows no overheating of the epoxy matrix.

Subsequent work will focus on extending and improving the drill cap avoidance process. The goal is a stiffness-independent process, where deflections of the workpiece (i.e. large wing parts) and the spindle (i.e. robot-based manufacturing) have no impact on the reliability of the process. This is an important step in developing a manufacturing instrument that is relevant to the aerospace industry. Tool life investigations as well as alternative cooling strategies (cryogenic machining) are planned to continue on the path towards “clean-one-shot-drilling”.

REFERENCES

- [1] Statista, *Use of materials in aircraft design 2014*, <https://www.statista.com/statistics/954913/share-composites-in-aircraft-design/?locale=en> (accessed Mar. 03, 2023).
- [2] BREUER U.P., 2016, *Commercial Aircraft Composite Technology*, New York, NY: Springer Berlin Heidelberg.
- [3] MEMON D.O., 2023. *Confusing Quantification: How Many Parts Does an Airliner Have?*, *Simple Flying*, <https://simpleflying.com/airliners-how-many-parts/> (accessed Apr. 06, 2023).
- [4] LIU D., TANG Y., CONG W.L., 2012, *A Review of Mechanical Drilling for Composite Laminates*, *Compos. Struct.*, 94/4, 1265–1279, <https://doi.org/10.1016/j.compstruct.2011.11.024>.
- [5] ZHU Z. et al., 2018, *Evaluation of Novel Tool Geometries in Dry Drilling Aluminium 2024-T351/Titanium Ti6Al4V Stack*, *J. Mater. Process. Technol.*, 259, 270–281, <https://doi.org/10.1016/j.jmatprotec.2018.04.044>.
- [6] PARK K.-H., BEAL A., KIM D.W., KWON P., LANTRIP J., 2011, *Tool Wear in Drilling of Composite/Titanium Stacks Using Carbide and Polycrystalline Diamond Tools*, *Wear*, 271/11–12, 2826–2835, <https://doi.org/10.1016/j.wear.2011.05.038>.
- [7] SENTHILKUMAR M., PRABUKARTHI A., KRISHNARAJ V., 2018, *Machining of CFRP/Ti6Al4V Stacks Under Minimal Quantity Lubricating Condition*, *J. Mech. Sci. Technol.*, 32/8, 3787–3796, <https://doi.org/10.1007/s12206-018-0731-6>.
- [8] HASSAN M.H., ABDULLAH J., MAHMUD A.S., SUPRAN A., 2017, *Burr Height as Quality Indicator in Single Shot Drilling of Stacked CFRP/Aluminium Composite*, *Key Eng. Mater.*, 744, 327–331, <https://doi.org/10.4028/www.scientific.net/KEM.744.327>.
- [9] BRINKSMEIER E., PECAT O., RENTSCH R., 2015, *Quantitative Analysis of Chip Extraction in Drilling of Ti6Al4V*, *CIRP Ann.*, 64/1, 93–96, <https://doi.org/10.1016/j.cirp.2015.04.064>.
- [10] NAN C., WU D., GAO Y., MA X., CHEN K., 2015, *Influence of Metal Chips on Drilling Quality of Carbon Fiber Reinforced Plastic and Titanium Stacks*, *IEEE International Conference on Cyber Technology in Automation, Control, and Intelligent Systems (CYBER)*, Shenyang, China: IEEE, 1204–1209, <https://doi.org/10.1109/CYBER.2015.7288115>.

- [11] LAPORTE S., De CASTELBAJAC C., LADONNE M., 2016, *Vibration Assisted Drilling on Automated Drilling Units: Challenges, Dynamic Modelization and Prospective Developments*, Aerospace Manufacturing and Automated Fastening Conference & Exhibition, SAE, <https://doi.org/10.4271/2016-01-2097>.
- [12] MUELLER-HUMMEL P., 2011, *New Solutions for one Shot Hand Held and Robot Drilling of CFRP/Titan and -/Aluminium Stack Drilling in H8 Quality for Aerospace Applications*, Aerospace Technology Conference and Exposition, <https://doi.org/10.4271/2011-01-2728>.
- [13] MUELLER-HUMMEL P., ATARSIA A., WIEMANN A., 2013, *One Shot - Dry - Drilling of Composites / Aluminium Hybrid Stacked Materials in IT8 Quality*, AeroTech Congress & Exhibition, SAE, <https://doi.org/10.4271/2013-01-2337>.
- [14] ASSADI M., MARTIN C., SIEGEL E., MATHIS D., 2013, *Body Join Drilling for One-Up-Assembly*, SAE Int. J. Aerosp., 6/1, 188–194, <https://doi.org/10.4271/2013-01-2296>.
- [15] DEVLIEG R. FEIKERT E., 2008, *One-Up Assembly with Robots*, SAE Whitepapers, <https://www.electroimpact.com/WhitePapers/2008-01-2297.pdf>.
- [16] LAPORTE S., De CASTELBAJAC C., 2012, *Major Breakthrough in Multi Material Drilling, Using Low Frequency Axial Vibration Assistance*, SAE Int. J. Mater. Manuf., 6/1, 11–18, <https://doi.org/10.4271/2012-01-1866>.
- [17] JALLAGEAS J., CHERIF M., J.-Y. K'NEVEZ, CAHUC O., 2013, *New Vibration System for Advanced Drilling Composite-Metallic Stacks*, SAE Int. J. Mater. Manuf., 7/1, 23–32, <https://doi.org/10.4271/2013-01-2078>.
- [18] LONFIER J., DE CASTELBAJAC C., 2014, *A Comparison Between Regular and Vibration-Assisted Drilling in CFRP/Ti6Al4V Stack*, SAE Int. J. Mater. Manuf., 8/1, 18–26, <https://doi.org/10.4271/2014-01-2236>.
- [19] De CASTELBAJAC C., LAPORTE S., LONFIER J., PUVILAND E., 2015, *A Global Improvement in Drilling and Countersinking of Multi-Material Stacks with Vibration Assisted Drilling*, SAE Int. J. Mater. Manuf., 9/1, 16–23, <https://doi.org/10.4271/2015-01-2501>.
- [20] PECAT O., PAULSEN T., KATTHÖFER, P., BRINKSMEIER E., FANGMANN S., 2016, *Vibration Assisted Drilling of Aerospace Materials*, Aerospace Manufacturing and Automated Fastening Conference & Exhibition, SAE, <https://doi.org/10.4271/2016-01-2136>.
- [21] PECAT O., BRINKSMEIER E., 2014, *Low Damage Drilling of CFRP/Titanium Compound Materials for Fastening*, Procedia CIRP, 13/1–7, <https://doi.org/10.1016/j.procir.2014.04.001>.
- [22] HUSSEIN R., SADEK A., ELBESTAWI M.A., ATTIA M.H., 2018, *Low-Frequency Vibration-Assisted Drilling of Hybrid CFRP/Ti6Al4V Stacked Material*, Int. J. Adv. Manuf. Technol., 98/9–12, 2801–2817, <https://doi.org/10.1007/s00170-018-2410-2>.
- [23] BLEICHER F., WIESINGER G., KUMPF C., FINKELDEI D., BAUMANN C., LECHNER C., 2018, *Vibration Assisted Drilling of CFRP/Metal Stacks at Low Frequencies and High Amplitudes*, Prod. Eng., 12/2, 289–296, <https://doi.org/10.1007/s11740-018-0818-z>.
- [24] BAI W., GAO Y., SUN R., 2023, *Vibration Assisted Machining: Fundamentals, Modelling and Applications*, Singapore, Springer.
- [25] ZHU Z., SUN X., GUO K., SUN J., LI J., 2022, *Recent Advances in Drilling Tool Temperature: A State-of-the-Art Review*, Chin. J. Mech. Eng., 35/1, 148, <https://doi.org/10.1186/s10033-022-00818-w>.
- [26] LTI Motion GMBH, 2016, *Documentation LeviSpin Vibrations-Bohrspindel*.
- [27] DEVLIEG R., SITTON K., FEIKERT E., INMAN J., 2002, *ONCE (ONE-sided Cell End effector) Robotic Drilling System*, Automated Fastening Conference & Exhibition, SAE, <https://doi.org/10.4271/2002-01-2626>.
- [28] SONNENBERG V., MEINHARD A., GÜTH S., 2017, *Gratminimales Bohren mit VHM-Bohrerkonzepten – ein Werkzeugbenchmark*, MM - Maschinenmarkt, [Online], <https://www.maschinenmarkt.vogel.de/gratminimales-bohren-mit-vhm-bohrerkonzepten-ein-werkzeugbenchmark-a-599508/>.
- [29] AMOYAL J., GARBER R., KARAMA M., KASSAHUN M., KOOHI A., 2015, *Design of an enhanced FOD inspection system for the aircraft assembly process*, Systems and Information Engineering Design Symposium, Charlottesville, VA, USA: IEEE, 142–147, <https://doi.org/10.1109/SIEDS.2015.7116963>.
- [30] DORNFELD D., MIN S., 2010, *A Review of Burr Formation in Machining*, in *Burrs - Analysis, Control and Removal*, J. C. Aurich and D. Dornfeld, Eds., Berlin, Heidelberg: Springer Berlin Heidelberg, 3–11, [Online], https://doi.org/10.1007/978-3-642-00568-8_1.
- [31] FELDSHTEIN E., 2011, *The Influence of Machining Conditions on Burr Shapes when Drilling Reach-Through Holes in Difficult-To-Cut Materials*, Adv. Manuf. Sci. Technol., 35, 75–83.
- [32] JAACKS K., 2016, *Automated Circumferential Joint Assembly in Aircraft Production - Development and Assessment of a Production Process*, Chalmers University of Technology, Gothenburg.
- [33] REITER M., BLEICHER F., 2019, *Affectation of Chip Formation in Single-Lip Deep Hole Drilling at Small Diameters by Application of Low-Frequency Vibration Support*, mm sci. j., 2019/04, 3107–3113, https://doi.org/10.17973/mmsj.2019_11_2019058.